Enhanced entanglement from Ince-Gaussian pump beams in spontaneous parametric down-conversion

Baghdasar Baghdasaryan ®* and Stephan Fritzsche ®

*Theoretisch-Physikalisches Institut, Friedrich-Schiller-Universität Jena, D-07743 Jena, Germany
and Helmholtz-Institut Jena, D-07743 Jena, Germany*

Spontaneous parametric down-conversion (SPDC) has been a reliable process for the generation of entangled photon pairs. In this process, a nonlinear quadratic crystal is pumped by a laser field in order to convert (high-energy) photons into correlated photon pairs whose efficient control plays an essential role in various applications of quantum information processing. In particular, the amount of entanglement has been successfully controlled by adjusting the spatial structure of the incident pump field. Here, we theoretically analyze how the entanglement of the down-converted two-photon state can be further enhanced by using Ince-Gaussian beams with well-defined *ellipticity* ϵ, i.e., solutions of the paraxial wave equation in elliptical coordinates. These spatially structured beams are quite universal as they include both the Laguerre-Gaussian beams for $\epsilon \to 0$ as well as the Hermite-Gaussian beams for $\epsilon \to \infty$. We demonstrate that the entanglement of the generated photon pairs in SPDC can be maximized by a proper choice of ϵ and that such an enhanced entanglement can be observed experimentally in terms of the Schmidt number.

I. INTRODUCTION

Entangled quantum states have been a crucial *resource* for various quantum applications, such as quantum cryptography [1], quantum teleportation [2], or quantum computing [3]. Therefore, until the present, many theoretical and experimental studies aim to find optimal or, at least, improved techniques to generate entangled states with high efficiency. Spontaneous parametric down-conversion (SPDC) is a robust experimental technique to generate two- or high-dimensional entangled states [4].

Indeed, SPDC is a widely applied nonlinear (optical) process that converts high-energy photons by a nonlinear birefringent crystal into entangled photon pairs. The down-converted photons can hereby be entangled in either their time bins [5], polarization [6,7], orbital angular momentum (OAM) [8–10], or with regard to their radial wave vector [11], in dependence of how the setup (geometry) is selected in a given experiment. It is therefore natural to ask how the state of the down-converted photons can be manipulated in order to enhance their entanglement. Apart from adjusting the properties of the crystal [11,12], the spatial structure of the incident pump beam can shape the two-photon state. For instance, an exponential pump beam has been used in order to flatten the OAM spectrum (spiral bandwidth) [13] or a superposition of Laguerre-Gaussian (LG) beams to generate a complete high-dimensional Bell basis [14]. In Sec. VI, we will discuss a few more articles in the context of our work.

In this article, we shall follow the last line and analyze how the pump beam can be controlled in order to improve the entanglement of the generated two-photon state. Along this line, previous works have considered as a pump beam, for instance, the paraxial Hermite-Gaussian (HG) [15,16] beams, Laguerre-Gaussian (LG) [17] beams, or a superposition of LG and HG beams [18]. HG and LG beams are well known as exact solutions for the free-space paraxial wave equation (PWE) in Cartesian and cylindrical coordinates. Here, we instead consider a more general paraxial pump field, also known as the Ince-Gaussian (IG) beam [19,20].

IG beams represent the exact, complete, and orthogonal solutions of the PWE in *elliptical* coordinates. Therefore, their transverse field distribution possesses an inherent elliptical symmetry. Experimentally, the IG beams appear naturally as transverse eigenmodes of stable resonators [21] but have been generated as well by means of liquid crystals [22]. The elliptical coordinates in the transverse plane $z = 0$ can be defined as $x = w_0(\epsilon/2)^{1/2} \cosh\xi \cos\eta$, $y = w_0(\epsilon/2)^{1/2} \sinh\xi \sin\eta$, where the parameter ϵ refers to the ellipticity and w_0 to the beam waist at the origin. The radial and angular elliptical coordinates are defined in the intervals $\xi \in [0, \infty)$ and $\eta \in [0, 2\pi)$, respectively. For a given beam waist w_0, each value of ϵ then specifies a different set of coordinates and, accordingly, different sets of IG modes. The elliptical coordinates (ξ, η) also include the Cartesian coordinates for $\epsilon \to 0$ as well as cylindrical coordinates for $\epsilon \to \infty$. Similarly, the IG beams include the LG beams ($\epsilon \to 0$) as well as the HG beams ($\epsilon \to \infty$). By just changing the ellipticity $0 \leqslant \epsilon \leqslant \infty$, one is therefore able to explore a whole *family* of beams, from the LG to the IG and up to the HG beams, respectively. We shall analyze in detail this beam dependence on the parameter ϵ as a technique for shaping the pump beam in the SPDC process.

In shaping the spatial structure of the incident beam, we may aim to either enhance (optimize) the strength of entanglement or the number of states (degrees of freedom), in which the down-converted two-photon state is entangled. For pure

*baghdasar.baghdasaryan@uni-jena.de

down-converted two-photon states, the amount of entanglement can be quantified in terms of the Schmidt number K by performing a Schmidt decomposition [3,23–25]. This decomposition naturally gives rise to a set of biorthogonal mode pairs in the representation of the bipartite states [26], while the Schmidt number refers to the average number of modes in the given state. In general, various approaches have been developed to experimentally detect and certify high-dimensional entangled states. For more details, we refer to a review article [27].

Below, we shall discuss both the numerical approach for calculating the Schmidt number (Sec. IV) as well as the role of Schmidt modes for the experiments. This includes a detailed discussion of the IG beams in Sec. II and of the SPDC state in Sec. III. Finally, an analysis is made for the Schmidt decomposition of the SPDC state for IG beams of a different kind in Sec. V.

II. INCE-GAUSSIAN BEAMS

An electromagnetic field is called *paraxial* if the ray inclination towards the optical axis is small. If a paraxial beam propagates along the z direction, its wave is given by $U = \Psi(\mathbf{r}) \exp{(ikz)}$ [28], and where the slowly varying amplitude Ψ satisfies the PWE,

$$\left(\nabla_\perp^2 + 2ik \frac{\partial}{\partial z} \right) \Psi(\mathbf{r}) = 0. \tag{1}$$

Here, $\nabla_\perp^2$ is the transverse Laplacian, $\mathbf{r}$ is the position vector, and k is the wave vector. The PWE has been solved in both Cartesian and cylindrical coordinates. We consider the solution of the PWE in elliptical coordinates, which is more general and includes the previously mentioned solutions in Cartesian and cylindrical coordinates.

A. PWE in elliptical coordinates

To obtain a solution of the PWE (1) in elliptical coordinates, let us consider an ansatz that is based on a lower-order Gaussian beam (GB),

$$\text{IG}(\mathbf{r}) = E(\xi) N(\eta) \exp{[iZ(z)]} \Psi_G(\mathbf{r}), \tag{2}$$

where $E(\xi)$, $N(\eta)$, and $Z(z)$ are assumed to be real functions, and where the GB itself satisfies the PWE,

$$\Psi_G(\mathbf{r}) = \frac{w_0}{w(z)} \exp\left[\frac{-r^2}{w^2(z)} + i \frac{kr^2}{2R(z)} - i\psi(z) \right].$$

In this (standard) definition of a GB, $w(z)^2 = w_0^2(1 + z^2/z_R^2)$ is the beam waist, $z_R = k w_0^2/2$ is the Rayleigh range, $R(z) = z + z_R^2/z$ is the radius of curvature of the phase front, $\psi(z) = \arctan(z/z_R)$ is the Gouy shift, and w_0 is the beam waist at the origin $z = 0$. Furthermore, if we insert the ansatz (2) into Eq. (1), one readily obtains three differential equations,

$$\frac{d^2E}{d\xi^2} - \epsilon \sinh(2\xi) \frac{dE}{d\xi} - [a - p\epsilon \cosh(2\xi)]E = 0, \tag{3}$$

$$\frac{d^2N}{d\eta^2} + \epsilon \sin(2\eta) \frac{dN}{d\eta} + [a - p\epsilon \cos(2\eta)]N = 0, \tag{4}$$

$$-\left(\frac{z^2 + z_R^2}{z_R} \right) \frac{dZ}{dz} = p, \tag{5}$$

with the two separation constants a and p, respectively. Together with the definition of a GB, the solutions of Eqs. (3)–(5) define the IG beams in elliptical coordinates. Indeed, Eq. (5) has a very simple solution $Z(z) = -p \arctan{(z/z_R)}$ that is known also as the *excess* phase. In contrast, Eqs. (3) and (4) require special care, as we shall briefly discuss below, and where the solution of Eq. (3) is obtained from (4) by replacing η with $i\xi$.

Since Eq. (4) represents (so-called) *periodic* differential equations, its solution must be also periodic. There are two independent solutions known as even and odd Ince polynomials of order p and degree m, denoted respectively as $C_p^m(\eta, \epsilon)$ and $S_p^m(\eta, \epsilon)$, where $0 \leqslant m \leqslant p$ for even, and $1 \leqslant m \leqslant p$ for odd functions. In both cases, moreover, p and m should obey the same parity rule: $(-1)^{(p-m)} = 1$. In the intensity distribution (cross section) of IG beams, the (quantum) number m refers to the number of hyperbolic nodal lines, while $(p - m)/2$ is the number of elliptic lines but without the line at $\xi = 0$ (see Fig. 1). In (quantum-) optical experiments, these quantum numbers are directly related to observables, such as the (projection of the) OAM and the radial wave vector (see Sec. II B).

The even and odd Ince polynomals are *periodic* and hence they can be expanded as a sum of finite trigonometric functions. There are four classes of Ince polynomials that are distinguished owing to their (anti)symmetry at $\eta = 0$ and $\eta = \pi/2$,

$$C_{2n}^{2k}(\eta, \epsilon) = \sum_{r=0}^{n} A_r^e \cos 2r\eta, \quad k = 0, \dots, n, \tag{6}$$

$$C_{2n+1}^{2k+1}(\eta, \epsilon) = \sum_{r=0}^{n} A_r^e \cos (2r + 1)\eta, \quad k = 0, \dots, n, \tag{7}$$

$$S_{2n}^{2k}(\eta, \epsilon) = \sum_{r=1}^{n} A_r^o \sin 2r\eta, \quad k = 1, \dots, n, \tag{8}$$

$$S_{2n+1}^{2k+1}(\eta, \epsilon) = \sum_{r=0}^{n} A_r^o \sin (2r + 1)\eta, \quad k = 0, \dots, n, \tag{9}$$

and where the superscripts e and o of the Fourier coefficients $A^{e,o}$ refer to *even* and *odd* Ince polynomials. By substituting expressions (6) into Eq. (4), these Fourier coefficients must obey the three-term recurrence relations

$$(p/2 + 1)\epsilon A_1^e = a A_0^e,$$
$$(p/2 + 2)\epsilon A_2^e = -p\epsilon A_0^e - (4 - a)A_1^e,$$
$$(p/2 + r + 2)\epsilon A_{r+2}^e = [a - 4(r + 1)^2]A_{r+1}^e + \left(r - \frac{p}{2} \right)\epsilon A_r^e,$$

with $r = 1, 2, \dots, n$. Similar three-term recurrence relations can be obtained also for the series (7)–(9) (for details, we refer to Ref. [20]). More generally, one should perform the following steps, in order to calculate the Fourier coefficients $A_r^{e,o}$: (i) Construct the coefficient matrix of the linear equation system which follows directly from the recurrence relations above. (ii) Find the real values of the parameter a, for which the coefficient matrix has nontrivial solutions (zero determinant): There are p such solutions for each m, a_p^m, and which can be arranged as $a_p^0 < a_p^1 < \dots < a_p^p$. (iii) For each value of
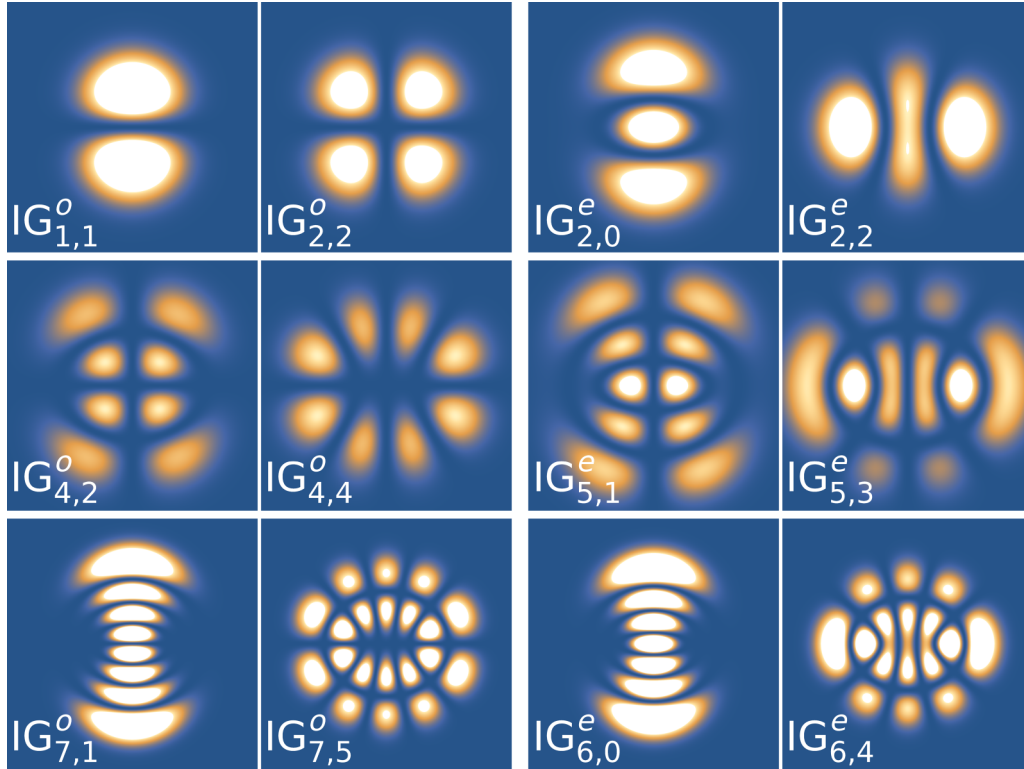
FIG. 1. Intensity profiles of odd and even IG beams in the transverse plane at $z = 0$ and for an ellipticity $\epsilon = 2$. The number of hyperbolic and elliptic nodal lines correspond to m and $(p - m)/2$, respectively, and without counting the interfocal nodal line at $\xi = 0$ for the odd modes.

a_p^m, one can solve the system of linear equations and find the corresponding set of coefficients $A_r^{e,o}$.

With these Fourier coefficients, we now can readily construct the three-dimensional solution, which should be continuous in the whole space. This continuity is ensured if the products of functions $E(\xi)$ and $N(\eta)$ in Eq. (2) have the same parity in ξ and η,

$$\mathrm{IG}_{p,m}^e(\mathbf{r}, \epsilon) = \frac{C w_0}{w(z)} C_p^m(i\xi, \epsilon) C_p^m(\eta, \epsilon) \exp\left[\frac{-r^2}{w^2(z)}\right]$$
$$\times \exp\left[ikz + \frac{ikr^2}{2R(z)} - (p+1)\psi(z)\right], \quad (10)$$

$$\mathrm{IG}_{p,m}^o(\mathbf{r}, \epsilon) = \frac{S w_0}{w(z)} S_p^m(i\xi, \epsilon) S_p^m(\eta, \epsilon) \exp\left[\frac{-r^2}{w^2(z)}\right]$$
$$\times \exp\left[ikz + \frac{ikr^2}{2R(z)} - (p+1)\psi(z)\right], \quad (11)$$

where C and S are two normalization constants. Figure 1 presents several transverse distributions of IG beams for the ellipticity $\epsilon = 2$ at $z = 0$.

To summarize this section, we see that the transverse distribution of IG beams at the beam waist plane is fully defined by the (quantum) numbers p and m as well as by the ellipticity ϵ and the beam waist w_0. This is a quite general result that each beam with well-defined spatial and spin properties can be characterized by just four parameters (quantum numbers), as all electrons or particles with well-defined spin; cf. the user guide to Ref. [29].

B. Relation between IG, LG, and HG beams

The IG beams exhibit an interesting property that is essential for our work below, and which refers to their limits of including both the LG or HG beams. Let us first write down the explicit expressions of these LG and HG modes in order to establish proper notations. The normalized LG modes are described by the radial number n and the OAM or winding number ℓ,

$$\mathrm{LG}_{n,\ell}^{e,o}(r, \phi, z) = \left[\frac{4n!}{(1 + \delta_{0,\ell})\pi(n + \ell)!}\right]^{1/2} \frac{1}{w(z)} \binom{\cos \ell\phi}{\sin \ell\phi}$$
$$\times \left[\frac{\sqrt{2}r}{w(z)}\right]^\ell L_n^\ell\left(\frac{2r^2}{w(z)^2}\right) \exp\left[\frac{-r^2}{w^2(z)}\right]$$
$$\times \exp\left\{i\left[kz + \frac{kr^2}{2R(z)} - (2n + \ell + 1)\psi(z)\right]\right\},$$
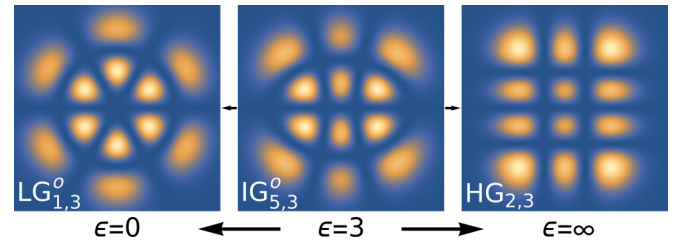

FIG. 2. The limit of the odd IG beam with $p = 5$ and $m = 3$ to the odd LG beam with $n = 1$ and $\ell = 3$ when the ellipticity goes to zero, as well as the limit to the HG beam with $n_x = 2$ and $n_y = 3$ when the ellipticity goes to infinity in Eqs. (10) and (11).

where $L_n^\ell(\cdot)$ are the generalized Laguerre polynomials. The normalized HG beams are instead described by the numbers n_x and n_y and are given by

$$
\begin{aligned}
\mathrm{HG}_{n_x,n_y}(x,y,z) = {} & \left[\frac{1}{2^{n_x+n_y-1}\pi\, n_x!\, n_y!}\right]^{1/2}\frac{1}{w(z)}H_{n_x}\!\left(\frac{\sqrt{2}x}{w(z)}\right)\\
& \times H_{n_y}\!\left(\frac{\sqrt{2}y}{w(z)}\right)\exp\left[\frac{-r^2}{w^2(z)}\right]\exp\left\{i\left[kz\right.\right.\\
& \left.\left.+\frac{kr^2}{2R(z)}-(n_x+n_y+1)\psi(z)\right]\right\},
\end{aligned}
$$

and where $H_n(\cdot)$ are the nth-order Hermite polynomials. The IG beams behave as LG modes when the ellipticity goes to zero, and where the following relations hold between the quantum numbers of the IG and LG modes: $m=\ell$, $p=2n+\ell$. Similarly, the IG beams behave as HG modes when the ellipticity goes to infinity. In the limit to HG modes, the conservation rules are denoted by $n_x=m-1$ and $n_y=p-m$ for even, and by $n_x=m-1$ and $n_y=p-m+1$ for odd IG beams; cf. Fig. 2.

The IG, LG, and HG modes each form a complete set of functions within the transverse plane and therefore can be expressed by each other. For example, an IG beam can be rewritten as a finite decomposition of LG beams as

$$
\mathrm{IG}_{p,m}^\sigma(\xi,\eta,\epsilon)=\sum_{n,\ell}D_{n,\ell}^\sigma\, LG_{n,\ell}^\sigma(r,\phi), \tag{12}
$$

where σ refers either to the even or to the odd beams, $\sigma=\{e,o\}$. Note that the expansion coefficients should be scaled out in order to hold the normalization condition $\sum_{n,\ell}D_{n,\ell}^2=1$. We can obtain these coefficient by performing the overlap integral between IG and LG beams,

$$
\begin{aligned}
\iint_{-\infty}^{\infty}\mathrm{LG}_{n,l}^\sigma\,\overline{\mathrm{IG}}_{p,m}^{\sigma'}dS = {} & \delta_{\sigma',\sigma}\,\delta_{p,2n+\ell}(-1)^{n+\ell+(p+m)/2}\\
& \times\sqrt{(1+\delta_{0,\ell})\Gamma(n+\ell+1)n!}\\
& \times A_{(\ell+\delta_{0,\sigma})/2}^\sigma(a_p^m),
\end{aligned}
$$

where $A_{(\ell+\delta_{0,\sigma})/2}^\sigma(a_p^m)$ are the Fourier coefficients from Eqs. (6)–(9), dS is the differential surface element, δ is the Kronecker delta function, and the overbar denotes the complex conjugate. The finite summation (12) runs up to $N_p=(p+2\delta_{\sigma,e})/2$ for even p, and up to $N_p=(p+1)/2$, for odd p. Let us make it explicit on an example. An odd IG beam with $p=5$ and ellipticity $\epsilon=2$ can be represented as a sum of three odd LG modes in the following way,

$$
\mathrm{IG}_{5,3}^o=-0.343\,\mathrm{LG}_{2,1}^o+0.901\,\mathrm{LG}_{1,3}^o+0.266\,\mathrm{LG}_{0,5}^o. \tag{13}
$$

Such a representation of the IG beams as a finite sum of LG modes has the great advantage that one can deal with cylindrical instead of elliptical coordinates.

C. Helical IG

Helical LG beams have a phase that rotates circularly about the propagation axis [30]. Similarly, one can also define helical IG (HIG) beams that exhibit elliptically rotating phases,

$$
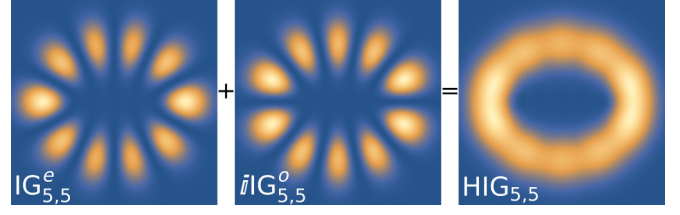\mathrm{HIG}_{p,m}=\mathrm{IG}_{p,m}^e\pm i\,\mathrm{IG}_{p,m}^o,
$$

FIG. 3. The construction of the helical IG beam as a sum of even and odd IG beams with ellipticity $\epsilon=2$. Obviously, the helical IG beam shows an elliptic ring structure.

where the sign defines the direction of the phase rotation. The HIG is defined only for $m>0$ since odd IG beams are not defined for $m=0$. Figure 3 illustrates the generation of a HIG beam as a linear sum of even and odd IG beams. In general, the number of elliptical rings is given by $1+(p-m)/2$, and a single ring just arises for $p=m$; cf. Fig. 3 with $p=m=5$.

III. SPONTANEOUS PARAMETRIC DOWN-CONVERSION

In typical SPDC experiments, a short quadratic nonlinear crystal is pumped with a strong (quasi)monochromatic laser that is assumed to propagate along the z axis. The efficiency for creating an SPDC pair of photons hereby depends on the conservation of energy and momentum, and which needs to be fulfilled for the SPDC process. While the energy conservation can be ensured by choosing narrow-band interference filters in front of the detectors, the momentum conservation is more difficult to fulfill with most materials. This momentum conservation can be realized using birefringent crystals that generally possess two or three different refractive indices for any given wavelength. However, nonideal conservation of the photon momenta should be taken into account when one wishes to derive an expression for the two-photon state.

For the sake of simplicity, we here assume the following for this derivation: (i) that the material is homogeneous and isotropic as justified for thin crystals; (ii) a collinear geometry of the generated photon pair with *zero* transverse component of the momentum vectors—this condition also ensures perfect phase matching between momentum vectors of down-converted photons; (iii) that the crystal is large enough in its transverse extent to absorb the whole pump beam; and that (iv) for a moderate pump laser, the (time) interval between subsequent down-conversions is much larger than the interaction time of the incident photon with the crystal and also when compared to the detection time. All these conditions can be readily fulfilled in experiments.

With these assumptions in mind, the generated two-photon state can be written as [31]

$$
|\Psi_{\mathrm{SPDC}}\rangle=\int d\boldsymbol{r}_\perp\Phi(\boldsymbol{r}_\perp)\hat{a}_s^\dagger(\boldsymbol{r}_\perp)\hat{a}_i^\dagger(\boldsymbol{r}_\perp)|00\rangle, \tag{14}
$$

where $\Phi(\boldsymbol{r}_\perp)$ is the spatial distribution of the pump beam at the input face of the crystal, $\boldsymbol{r}_\perp$ is the radial coordinate in real space, $\hat{a}_s^\dagger(\boldsymbol{r}_\perp)$ and $\hat{a}_i^\dagger(\boldsymbol{r}_\perp)$ are the creation operators for the signal and idler photons and, respectively, $|00\rangle$ the *vacuum* state.

The subscripts s and i refer to the two down-converted *signal* and *idler* photons, respectively. Although this expression (14) appears to be quite simple, it has been found useful to describe a good number of experimental results [32].

To explore the spatial structure of the down-converted state, we need to perform a mode decomposition of the joint wave function (14). This is achieved by using a complete and orthogonal basis of transverse optical modes, and has been previously done by using Bessel [11], HG [15,25,33,34], LG [35,36], or IG modes [37]. Here, we shall choose the LG modes as a basis for this decomposition because of the following two reasons: First, the down-converted photons are naturally entangled in the arbitrary superpositions of the OAM modes as it was demonstrated theoretically [8,9] and experimentally [10]. Second, the spatial modes may carry and are often classically correlated with regard to their radial momentum vector [35,38]. Moreover, the first experimental realization of high-dimensional entanglement consisting of radial modes has been introduced in Ref. [39], where 100-dimensional entanglement of a two-photon system has been detected by utilizing a modified measurable witnesslike quantity. The OAM and the radial momentum vector can be well described by the discrete OAM and radial numbers of LG modes. Therefore, the use of LG modes in the decomposition above will simplify the mathematical treatment and calculation of the SPDC state.

A single photon in an LG mode can be written as

$$|n, \ell\rangle = \int d\boldsymbol{r}_\perp \mathrm{LG}_{n,\ell}(\boldsymbol{r}_\perp), \hat{a}^\dagger(\boldsymbol{r}_\perp) |0\rangle, \quad (15)$$

where we use the helical LG modes in real space:

$$\mathrm{LG}_{n,\ell}(r, \phi) = \sqrt{\frac{2n!}{\pi(n+|\ell|)}} \frac{1}{w} \left(\frac{r\sqrt{2}}{w}\right)^{|\ell|}$$
$$\times \exp\left(\frac{-r^2}{w^2}\right) L_n^{|\ell|}\left(\frac{2r^2}{w^2}\right) \exp(i\ell\phi).$$

With this notation, the expansion of the SPDC state (14) in terms of LG modes is then given by

$$|\Psi_{\mathrm{SPDC}}\rangle = \sum_{n_s, \ell_s} \sum_{n_i, \ell_i} C_{n_s, n_i}^{\ell_s, \ell_i} |n_s \ell_s; n_i \ell_i\rangle. \quad (16)$$

Using Eqs. (14)–(16), the expansion coefficients are obtained from

$$C_{n_s,n_i}^{\ell_s,\ell_i} = \int d\boldsymbol{r}_\perp \Phi(\boldsymbol{r}_\perp)[\mathrm{LG}_{n_s,\ell_s}(\boldsymbol{r}_\perp)]^*[\mathrm{LG}_{n_i,\ell_i}(\boldsymbol{r}_\perp)]^*. \quad (17)$$

If we substitute expression (12) of the IG beam for the pump field $\Phi(\boldsymbol{r}_\perp)$, the expansion coefficients (17) can be evaluated analytically. For an odd, even, and helical IG pump beam, these coefficients read as

$$O_{n_s,n_i}^{\ell_s,\ell_i} = \sum_{n,\ell} \frac{i}{2} D_{n,\ell}^o \big(\delta_{-\ell,\ell_s+\ell_i} - \delta_{\ell,\ell_s+\ell_i}\big) B_{n,n_s,n_i}^{\ell,\ell_s,\ell_i}, \quad (18)$$

$$E_{n_s,n_i}^{\ell_s,\ell_i} = \sum_{n,\ell} \frac{1}{2} D_{n,\ell}^e \big(\delta_{-\ell,\ell_s+\ell_i} + \delta_{\ell,\ell_s+\ell_i}\big) B_{n,n_s,n_i}^{\ell,\ell_s,\ell_i}, \quad (19)$$

$$H_{n_s,n_i}^{\ell_s,\ell_i} = E_{n_s,n_i}^{\ell_s,\ell_i} + iO_{n_s,n_i}^{\ell_s,\ell_i}, \quad (20)$$

with

$$B_{n,n_s,n_i}^{\ell,\ell_s,\ell_i} = \sqrt{\frac{2}{\pi w_p^2} \frac{2^{\sigma_\ell+1}\gamma_s^{|\ell_s|+1}\gamma_i^{|\ell_i|+1}}{(1+\gamma_s^2+\gamma_i^2)^{\sigma_\ell+1}}} \sqrt{n!n_s!n_i!(|\ell|+n)!(|\ell_s|+n_s)!(|\ell_i|+n_i)!}$$
$$\times \sum_{k=0}^{n} \sum_{i=0}^{n_s} \sum_{j=0}^{n_i} \frac{(-2)^{k+i+j}\gamma_s^{2i}\gamma_i^{2j}(\sigma_\ell+k+i+j)!}{(1+\gamma_s^2+\gamma_i^2)^{k+i+j}(n-k)!(|\ell|+k)!k!(n_s-i)!(|\ell_s|+i)!i!(n_i-j)!(|\ell_i|+j)!j!},$$

and where we used the notation $\sigma_l = (|\ell_p| + |\ell_s| + |\ell_i|)/2$. Moreover, the ratios of the pump width to the signal and idler widths are denoted by $\gamma_s = w_p/w_s$ and $\gamma_i = w_p/w_i$.

IV. SCHMIDT BASES FOR THE DOWN-CONVERTED PHOTONS

Let us first recall the Schmidt decomposition of an (entangled) pure bipartite state from a mathematical viewpoint. If we consider the two subsystems A and B with Hilbert spaces H_A and H_B, any pure state of the composite system AB can be written as

$$|\psi\rangle = \sum_{a,b} \psi_{ab} |a\rangle \otimes |b\rangle \quad \in H_A \otimes H_B, \quad (21)$$

where the vectors $\{|a\rangle\}$ and $\{|b\rangle\}$ represent the bases for the Hilbert spaces H_A and H_B, respectively. We can use the singular value decomposition (SVD) theorem in order to write the coefficients matrix of the state $|\psi\rangle$ in the form

$$\psi = U \Lambda V^\dagger, \quad (22)$$

where the matrices U and V have *orthogonal columns*, $U^\dagger U = 1$ and $V^\dagger V = 1$, and where the matrix Λ is diagonal with entries $\Lambda_{kk} = \lambda_k$. These diagonal (matrix) elements are also known as the singular values of the matrix ψ, while the number of nonzero singular values is called the *Schmidt rank* of the matrix. From Eq. (22), it then follows that the state (21) can be represented as [3]

$$\psi_{ab} = \sum_k^r \lambda_k U_{ak} V_{bk}^*, \quad (23)$$

where r is the Schmidt rank. We can now insert the coefficients ψ_{ab} back into Eq. (21),

$$|\psi\rangle = \sum_{a,b,k} \lambda_k U_{ak} V_{bk}^* |a\rangle \otimes |b\rangle$$
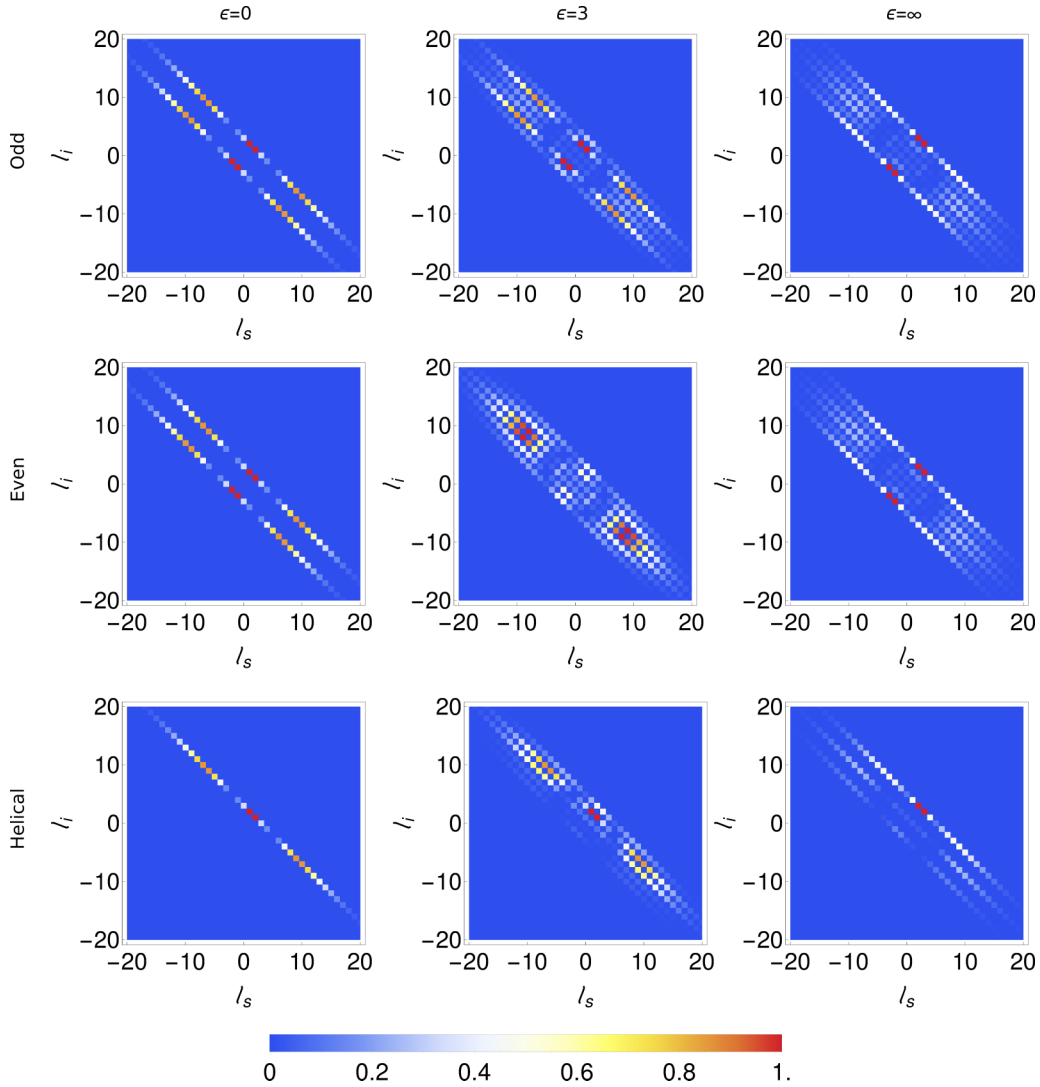$$= \sum_k \lambda_k \left[\sum_a U_{ak} |a\rangle\right] \otimes \left[\sum_b V_{bk}^* |b\rangle\right],$$

FIG. 4. Correlation between the OAMs ℓ_s and ℓ_i of signal and idler photons for an IG pump beams with $p = 5$, $m = 3$, $w_p = 1$, and ellipticities, $\epsilon = 0$, 3, and ∞. Here, we assume that the pump, signal, and idler beams all have the same widths, $\gamma_s = \gamma_i = 1$. For an IG pump beam with $p = 5$, one generally expects six *lines* with total OAM $\ell_s + \ell_i = \pm 1, \pm 3, \pm 5$. In the limit of a helical LG beam, the pump beam possesses a well-defined OAM. Therefore, one expects only a single line with $\ell = m = 3$. All figures are calculated for the fundamental modes $p_s = p_i = 0$, while the normalization is done for each graph individually.

and introduce the two bases, $|u_k\rangle_a = \sum_a U_{ak} |a\rangle$ and $|u_k\rangle_b = \sum_b V_{bk}^* |b\rangle$, to finally obtain

$$|\psi\rangle = \sum_k \lambda_k |u_k\rangle_a |u_k\rangle_b. \qquad (24)$$

Expression (24) is known in the literature as the Schmidt decomposition of the initial state (21) with $|u_k\rangle_a$ and $|u_k\rangle_b$ being the Schmidt modes and λ_k the corresponding eigenvalues. The Schmidt decomposition of pure bipartite states has several interesting properties that make it an attractive tool for both experimental and theoretical investigations: (i) The Schmidt modes form a complete and orthogonal basis. (ii) The Schmidt modes provide a discrete single-sum representation, independent of the particular state. (iii) The Schmidt number $K = 1/\sum_k \lambda_k^4$ quantifies the amount of entanglement if the state $|\psi\rangle$ is normalized: $\sum_k \lambda_k^2 = 1$. The more the probabilities λ_k are distributed, the more is

the state entangled. In particular, the state $|\psi\rangle$ is separable for the Schmidt number $K = 1$ and is called entangled for $K > 1$. The Schmidt number is generally not bounded from above.

There are noticeable differences for the decomposition of the SPDC state $|\Psi_{\text{SPDC}}\rangle$ in terms of LG and Schmidt modes. In particular, the LG modes (16) are not suitable as a measurement basis since each LG mode of one of the photons is generally correlated with several radial modes of the other photon. Such correlations are very different for the Schmidt decomposition (24) for which a *postmeasurement* state $|u_k\rangle_a$ of subsystem A implies (ideally) to find subsystem B in the state $|u_k\rangle_b$. In the Schmidt basis, therefore, all measurements on A and B are perfectly correlated. Moreover, if the measurement basis differs from the Schmidt basis, the obtained (effective) Schmidt number will always be smaller than those in the Schmidt basis.
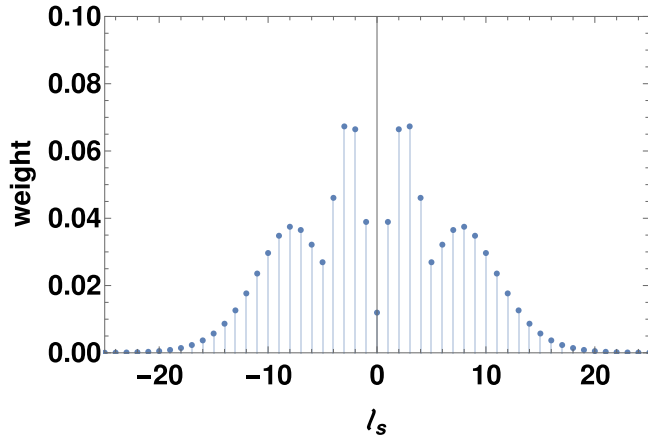
FIG. 5. Spiral bandwidth of the SPDC state if the pump field is an odd IG beam with $p = 5$, $m = 5$, and $\epsilon = 3$. Each point correspond to superposition of all states with fixes ℓ_s.
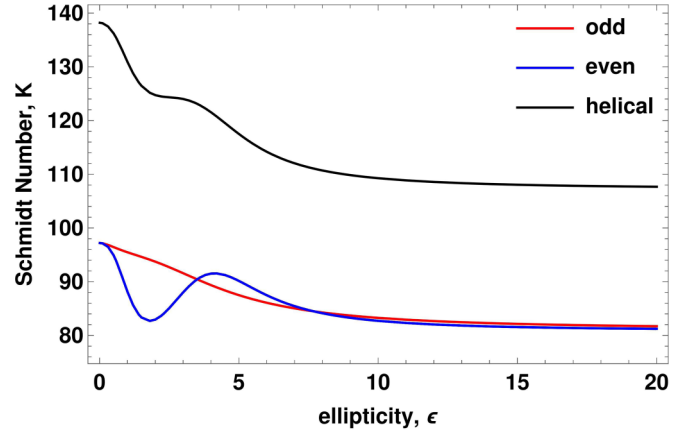

FIG. 6. Dependence of the Schmidt number on the ellipticity of the incident IG beam. The two-photon state has been constructed by considering the significant terms of the sum (16). Odd, even, and helical IG pump beams are denoted by red, dashed blue, and black lines, respectively.

V. INVESTIGATION OF THE SPDC STATE

Expressions (18)–(20) describe the spatial structure of the SPDC state in terms of LG modes for different kinds of IG pump fields (beams). These decompositions of the pump field depend, of course, on the particular parameters of the incident beam, such as its ellipticity, width, and quantum numbers, as well as on the widths of the signal and idler beams. Below, we shall explore (incident) paraxial pump beams with different ellipticities, including LG, IG, and HG beams. We shall also discuss how (entanglement) measurements can be implemented experimentally and which correlation distributions we expect for the different input beams.

A. Correlation between OAM of signal and idler photons

The SPDC process generally conserves the OAM of the incident beam as known from theory and experiments. If a nonlinear crystal is pumped by a pure helical LG beam with OAM ℓ_p, the output state has a total OAM $\ell_s + \ell_i = \ell_p$ with the OAMs of the signal (ℓ_s) and idler photons (ℓ_i), respectively. Let us start with an odd LG pump beam. Since an odd LG beam can be represented as a sum of two helical LG beams, the generated photon pair will have a total OAM either ℓ_p or $-\ell_p$ with the same probability, $\ell_s + \ell_i = \pm\ell_p$. Especially, an odd IG pump beam with $p = 5$ can be expressed as the sum of three LG beams with OAMs $\ell = 1$, 3, and 5 [see Eq. (13)], which implies that the down-converted photons can possess a total OAM of $\ell_s + \ell_i = \pm 1, \pm 3, \pm 5$. Figure 4 shows the conservation of the OAM in the SPDC process if the crystal is pumped by an IG beam with $p = 5$ and $m = 3$. As expected, an IG pump beam (middle column) shows six *lines* with total OAM $\ell_s + \ell_i = \pm 1 \pm 3 \pm 5$. From these lines, only *two* remain for all even and odd IG beams in the limit $\epsilon \to 0$, while just a single line remains for a helical LG beam with $\ell = m = 3$. The helical HG modes are obtained from the HIG beams in the limit $\epsilon \to \infty$. In general, the modes with a negative total OAM are suppressed for the helical beams (lower panel of Fig. 4). In addition, the correlation between the OAMs ℓ_s and ℓ_i also depends on the width ratios γ_s and γ_i

as well as the mode number m, though this dependence is not shown here.

B. Spiral bandwidth of the SPDC state

The *spiral* bandwidth has been used in the literature to describe the degree of entanglement, namely the number of OAM modes that contribute to the state. The spiral bandwidth is therefore directly related to the number of entangled modes. If, moreover, this bandwidth describes an equally distributed multimode expansion, the corresponding state is maximally entangled. Therefore, an interesting question of current research is how these spiral bandwidths can be manipulated. Figure 5 shows the spiral bandwidth for an odd IG pump beam with $p = 5$, $m = 3$, and $\epsilon = 3$. Each point in Fig. 5 represents the sum over all possible OAM states for a fixed ℓ_s and for the fundamental modes with $n_s = n_i = 0$ from expression (16).

In a series of test computations, we also analyzed how the spiral bandwidth depends on the ellipticity parameter. In practice, however, this dependence is difficult to interpret and will not be shown explicitly. Instead, we here display how the Schmidt number as *one* observable of SPDC experiments depends on the ellipticity of the incident beam.

C. Schmidt number of the SPDC state

As mentioned before, the Schmidt number characterizes the amount of entanglement. Here, we shall therefore investigate how this number depends on the ellipticity of the (incident) IG beam. A full representation of the down-converted photon state is obtained in expression (16) when $\ell_{s,i}$ run overall integers, while $n_{s,i}$ only over the positive integers. For the sake of simplicity, we here considered only the most significant terms in the sum (16), i.e., we restrict ourselves to the radial numbers $n = 0, 1, \ldots, 10$ and to the OAM $\ell = -25, -24, \ldots, 24, 25$. This restriction is still a very good approximation to the real photon state since all higher-order coefficients (17) are significantly smaller. We used the method from Sec. IV and constructed a coefficient matrix similar to
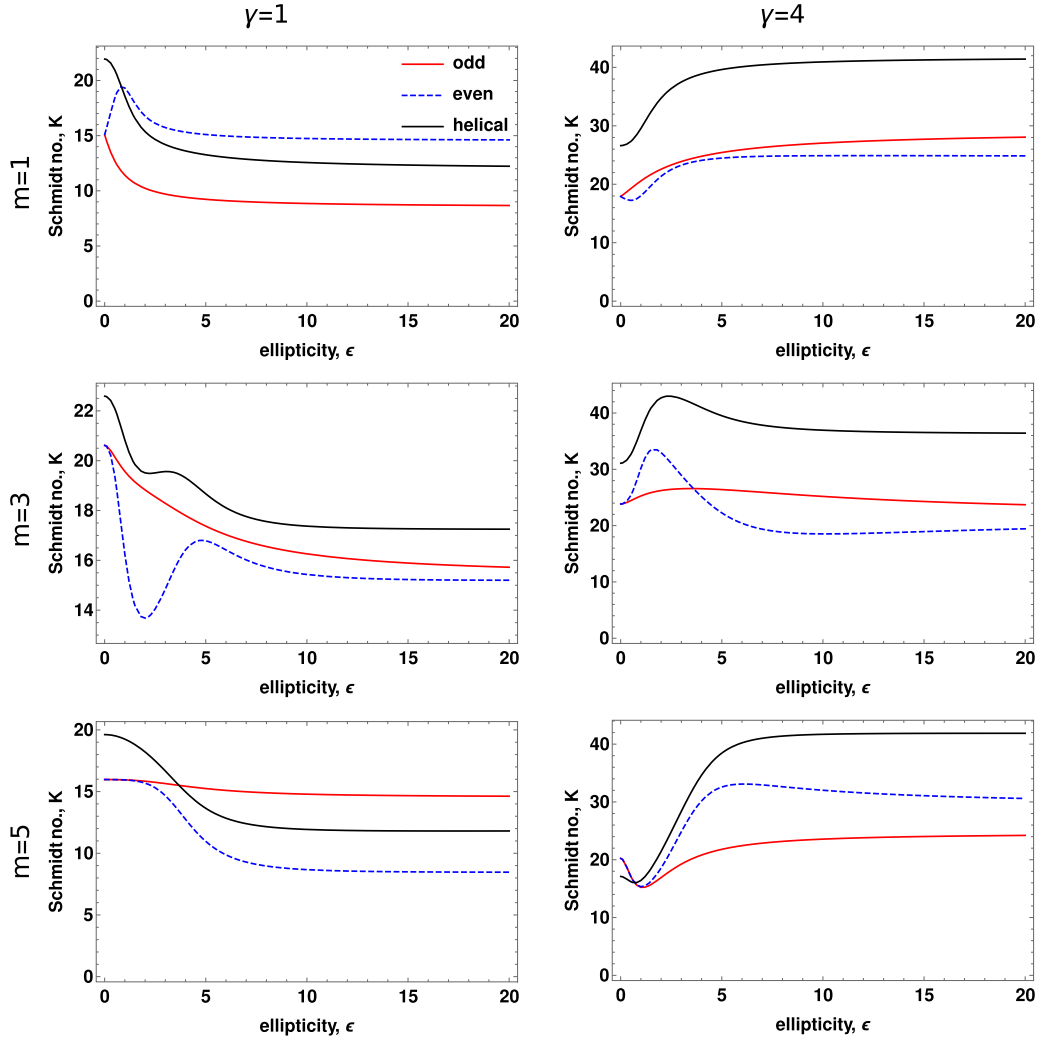
FIG. 7. The same as Fig. 6 but for different ratios of the widths of the pump, signal, and idler beams, $\gamma = \gamma_s = \gamma_i = 1$ and 4, as well as for different mode numbers m of IG pump beams of different kinds with $p = 5$. The curves of helical and even beams behave similarly for $\gamma = 1$: The maximum Schmidt number is reached in the limit of a pure LG beam, and it decreases when the ellipticity increases up to the limit of an HG beam. The curve for an even beam with $m = 1$ shows a maximum for an IG mode between LG and HG modes. Depending on the incident light's mode number, the curves can have a maximum in the limit of HG beams if the ratio of the beam widths becomes larger than one, $\gamma > 1$. Although all curves have been calculated for the fundamental modes $n = 0$, their dependence on the ellipticity ϵ will remain unchanged if we also consider the radial modes.

Eq. (23). The Schmidt number has been calculated by using the SVD method described in Sec. IV.

Figure 6 shows the dependence of the Schmidt number on the ellipticity, when the pump beam is an IG with $p = 5$ and $m = 3$ and where beam widths are chosen to be equal, $\gamma_s = \gamma_i = \gamma = 1$. The proper choice of the kind (odd, even, or helical) and ellipticity can maximize the amount of entanglement. While Fig. 6 implies only a rather weak dependence on the ellipticity, this changes if we consider the full state for which the differences between the maximum and minimum become significant.

We also investigated the Schmidt number for pure OAM modes with fixed radial modes, $n_s = n_i = 0$. Figure 7 shows the dependence of the Schmidt number on the ellipticity parameter; in particular, we here fixed the order $p = 5$ of the pump beam and varied the mode number m as well as the ratios of the pump-to-signal and pump-to-idler widths.

Obviously, the curves behave quite differently for different sets of beam parameters. The maximum Schmidt number is achieved in the LG limit ($\epsilon \to 0$), if the pump beam is an odd or helical IG beam, and if all three beams are equal: $\gamma_s = \gamma_i = 1$. We can see from Fig. 7 that a maximum can be reached also for an IG beam with finite $\epsilon > 0$ but only for particular parameters. We realize from the comparison of Fig. 6 with its analog from Fig. 7, that the curve's behavior is independent of how many radial modes are involved in the state, i.e., the ellipticity dependence is relevant only for OAM modes.

D. Experimental model

Spatial light modulators (SLMs) are often used to generate or detect the spatial modes of light beams. Such SLMs can readily transform a particular spatial mode into a fundamental Gaussian mode, and which can then be coupled into the
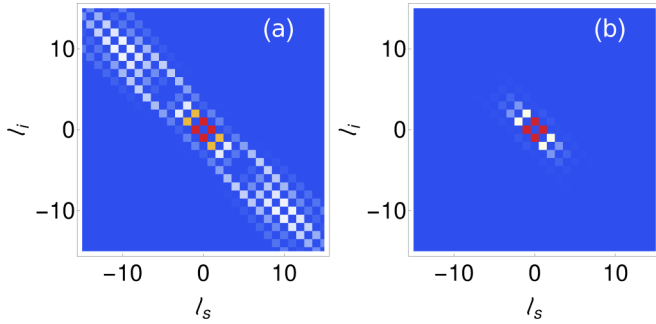
FIG. 8. The same as Fig. 4 but for $\gamma_s = \gamma_i = \gamma_0 = 2$, where γ_0 is the ratio of the pump width to the single-mode fiber width, $\gamma_0 = w_p/w_0$. A realistic single-mode fiber affects the spiral bandwidths; since these fibers have a finite size, not all generated Gaussian modes can be coupled into it equally.

single-mode fiber. These SLMs can be applied also in order to perform coincidence detections of down-converted photons [10,11]. Since the single-mode fibers have a finite size, they cannot couple all Gaussian modes. Therefore, one may better consider an additional Gaussian mode in Eq. (14) in order to model such an experiment [32],

$$|\Psi_{\text{SPDC}}\rangle = \int d\boldsymbol{r}_\perp \Phi(\boldsymbol{r}_\perp) \hat{a}_s^\dagger(\boldsymbol{r}_\perp) \hat{a}_i^\dagger(\boldsymbol{r}_\perp) G^2(\boldsymbol{r}_\perp) |00\rangle, \quad (25)$$

where the Gaussian mode of a single-mode fiber with a radius w_0 can be written as

$$G(\boldsymbol{r}_\perp) = \left(\frac{2}{\pi}\right)^{1/2} \frac{1}{w_0} \exp\left(-\frac{\boldsymbol{r}_\perp^2}{w_0^2}\right).$$

Here, the additional term in Eq. (25) can be interpreted as an adjustment of the beam waist of the pump beam. From Eqs. (10) or (11), we see indeed that the beam waist can be adjusted in the following way,

$$\frac{1}{(w_p')^2} = \frac{1}{w_p^2} + \frac{2}{w_0^2},$$

where w_p' is the effective beam width. Figure 8 presents the differences of the spiral bandwidths and the Schmidt number distributions, if one considers the effective beam waist. From Fig. 8, we finally see that the spiral bandwidths decrease because not all modes can be coupled into the single-mode fiber. This also affects the Schmidt number distributions from Figs. 6 and 7, which are not presented here, but should be considered for modeling the real experiment outcomes.

VI. COMPARISON WITH PREVIOUS WORKS

A superposition of LG beams has been used as a pump beam in order to generate high-dimensional entangled states [40,41]. In these works, for instance, a superposition of three LG beams has been utilized to generate three-dimensional maximally entangled states. Analogously, IG beams can be utilized to generate high-dimensional entangled states by adjusting the ellipticity. Such an IG beam with quantum numbers $p = 5$ and $m = 1$ generates a four-dimensional maximally entangled state for ellipticity, $\varepsilon = 1.08$ in the subspace $\ell =$
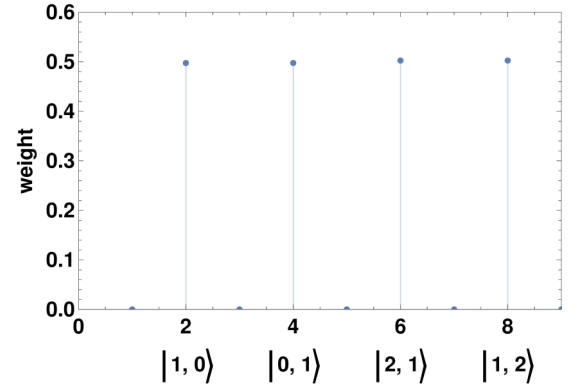

FIG. 9. Generation of a four-dimensional maximally entangled state in the subspace $\ell = 0, \pm 1, \pm 2$ and $n = 0$. The pump beam is a helical IG beam with $p = 5$ and $m = 1$ and with ellipticity $\varepsilon = 1.08$.

$0, \pm 1, \pm 2$ and $n = 0$ (see Fig. 9). On the other hand, IG beams can be also represented as a superposition of LG beams [see Eq. (13)], which implies that our approach is similar to the methods from Refs. [40,41]. The crucial difference is that this superposition refers to a certain ellipticity parameter, which is a unique feature of IG beams. Moreover, this additional information regarding the ellipticity can be transferred in the SPDC process to the state of down-converted photons. In order to verify this, we consider an IG pump beam with ellipticity, $\varepsilon = 2$, and analyze the correlation between two down-converted photons when projected onto IG modes with the same mode numbers. Figure 10 shows the correlation strength depending on the ellipticity of down-converted photons. As we can see, the correlation reaches the maximum value when the ellipticities of the pump and down-converted beams are equal, otherwise, the correlation is reduced. Hence, the ellipticity can be used for extensions of quantum communication protocols such as the Bennett-Brassard protocol of 1984 (BB84) or the Ekert protocol of 1991 (Ekert91), for instance, as an encoded parameter. With
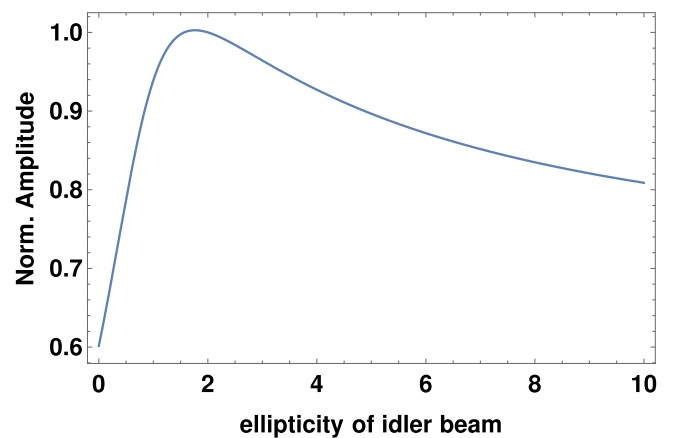

FIG. 10. Strength of correlation depending on the ellipticity of the idler beam, when the pump beam is an IG beam with $\varepsilon = 2$. Idler and signal beams are projected into IG modes with the same mode numbers. The maximum correlation is reached when the ellipticities of the pump and down-converted beams are equal.

this in mind, the ellipticity of IG beams gives a different physical meaning to the superposition of LG beams used in SPDC.

VII. CONCLUSION

In this article, we explore the state of (spontaneous parametric) down-converted photons $|\Psi_{SPDC}\rangle$ for different Ince-Gaussian (IG) pump beams and their different limits. Our goal was to investigate the SPDC process for general paraxial pump fields, the (so-called) IG beam from which both the

paraxial LG are obtained for a zero ellipticity $\varepsilon \to 0$ as well as the HG beams for $\varepsilon \to \infty$. Therefore, the shape of the pump beam is easily controlled using the ellipticity parameter. We show how the entanglement of the SPDC two-photon states can be maximized by a proper choice of the ellipticity ε. We also show how the Schmidt number as an observable of such SPDC experiments can be utilized to better understand the amount of (generated) entanglement. The smooth transition of IG beams into LG beams has been analyzed in terms of the spiral bandwidth and the conservation (rule) of the OAM in the SPDC process.

[1] R. Ursin, F. Tiefenbacher, T. Schmitt-Manderbach, H. Weier, T. Scheidl, M. Lindenthal, B. Blauensteiner, T. Jennewein, J. Perdigues, P. Trojek, B. Ömer, M. Fürst, M. Meyenburg, J. Rarity, Z. Sodnik, C. Barbieri, H. Weinfurter, and A. Zeilinger, Nat. Phys. **3**, 481 (2007).

[2] D. Bouwmeester, J.-W. Pan, K. Mattle, M. Eibl, H. Weinfurter, and A. Zeilinger, Nature (London) **390**, 575 (1997).

[3] M. A. Nielsen and I. L. Chuang, *Quantum Computation and Quantum Information: 10th Anniversary Edition*, 10th ed. (Cambridge University Press, New York, 2011).

[4] C. K. Hong and L. Mandel, Phys. Rev. A **31**, 2409 (1985).

[5] P. R. Tapster, J. G. Rarity, and P. C. M. Owens, Phys. Rev. Lett. **73**, 1923 (1994).

[6] P. G. Kwiat, K. Mattle, H. Weinfurter, A. Zeilinger, A. V. Sergienko, and Y. Shih, Phys. Rev. Lett. **75**, 4337 (1995).

[7] P. G. Kwiat, E. Waks, A. G. White, I. Appelbaum, and P. H. Eberhard, Phys. Rev. A **60**, R773 (1999).

[8] H. H. Arnaut and G. A. Barbosa, Phys. Rev. Lett. **85**, 286 (2000).

[9] S. Franke-Arnold, S. M. Barnett, M. J. Padgett, and L. Allen, Phys. Rev. A **65**, 033823 (2002).

[10] A. Mair, A. Vaziri, G. Weihs, and A. Zeilinger, Nature (London) **412**, 313 (2001).

[11] B. Baghdasaryan, F. Steinlechner, and S. Fritzsche, Phys. Rev. A **101**, 043844 (2020).

[12] R. Ramirez-Alarcon, H. Cruz-Ramirez, and A. U'Ren, Laser Phys. **23**, 055204 (2013).

[13] S. Liu, Y. Zhang, C. Yang, S. Liu, Z. Ge, Y. Li, Y. Li, Z. Zhou, G. Guo, and B. Shi, Phys. Rev. A **101**, 052324 (2020).

[14] Y. Chen, W. Zhang, D. Zhang, X. Qiu, and L. Chen, arXiv:2006.00445.

[15] S. P. Walborn and A. H. Pimentel, J. Phys. B: At., Mol. Opt. Phys. **45**, 165502 (2012).

[16] S. P. Walborn and C. H. Monken, Phys. Rev. A **76**, 062305 (2007).

[17] A. M. Yao, New J. Phys. **13**, 053048 (2011).

[18] J. P. Torres, Y. Deyanova, L. Torner, and G. Molina-Terriza, Phys. Rev. A **67**, 052313 (2003).

[19] M. A. Bandres and J. C. Gutiérrez-Vega, Opt. Lett. **29**, 144 (2004).

[20] M. A. Bandres and J. C. Gutiérrez-Vega, J. Opt. Soc. Am. A **21**, 873 (2004).

[21] U. T. Schwarz, M. A. Bandres, and J. C. Gutiérrez-Vega, Opt. Lett. **29**, 1870 (2004).

[22] J. B. Bentley, J. A. Davis, M. A. Bandres, and J. C. Gutiérrez-Vega, Opt. Lett. **31**, 649 (2006).

[23] F. M. Miatto, H. Di Lorenzo Pires, S. M. Barnett, and M. P. van Exter, Eur. Phys. J. D **66**, 263 (2012).

[24] F. M. Miatto, T. Brougham, and A. M. Yao, Eur. Phys. J. D **66**, 183 (2012).

[25] S. S. Straupe, D. P. Ivanov, A. A. Kalinkin, I. B. Bobrov, and S. P. Kulik, Phys. Rev. A **83**, 060302(R) (2011).

[26] C. K. Law, I. A. Walmsley, and J. H. Eberly, Phys. Rev. Lett. **84**, 5304 (2000).

[27] N. Friis, G. Vitagliano, M. Malik, and M. Huber, Nat. Rev. Phys. **1**, 72 (2019).

[28] B. Baghdasaryan, B. Böning, W. Paufler, and S. Fritzsche, Phys. Rev. A **99**, 023403 (2019).

[29] S. Fritzsche, Comput. Phys. Commun. **240**, 1 (2019).

[30] L. Allen, M. W. Beijersbergen, R. J. C. Spreeuw, and J. P. Woerdman, Phys. Rev. A **45**, 8185 (1992).

[31] B. E. A. Saleh, A. F. Abouraddy, A. V. Sergienko, and M. C. Teich, Phys. Rev. A **62**, 043816 (2000).

[32] Y. Zhang, F. S. Roux, M. McLaren, and A. Forbes, Phys. Rev. A **89**, 043820 (2014).

[33] S. P. Walborn, S. Pádua, and C. H. Monken, Phys. Rev. A **71**, 053812 (2005).

[34] X.-F. Ren, G.-P. Guo, J. Li, and G.-C. Guo, Phys. Lett. A **341**, 81 (2005).

[35] F. M. Miatto, A. M. Yao, and S. M. Barnett, Phys. Rev. A **83**, 033816 (2011).

[36] J. P. Torres, A. Alexandrescu, and L. Torner, Phys. Rev. A **68**, 050301(R) (2003).

[37] M. Krenn, R. Fickler, M. Huber, R. Lapkiewicz, W. Plick, S. Ramelow, and A. Zeilinger, Phys. Rev. A **87**, 012326 (2013).

[38] V. D. Salakhutdinov, E. R. Eliel, and W. Löffler, Phys. Rev. Lett. **108**, 173604 (2012).

[39] M. Krenn, M. Huber, R. Fickler, R. Lapkiewicz, S. Ramelow, and A. Zeilinger, Proc. Natl. Acad. Sci. USA **111**, 6243 (2014).

[40] E. V. Kovlakov, S. S. Straupe, and S. P. Kulik, Phys. Rev. A **98**, 060301(R) (2018).

[41] S. Liu, Z. Zhou, S. Liu, Y. Li, Y. Li, C. Yang, Z. Xu, Z. Liu, G. Guo, and B. Shi, Phys. Rev. A **98**, 062316 (2018).